Y.X. Xu, Y.L. Wang and C.L. Zeng*

Electrochemical Studies of the Corrosion of Pure Fe, Ni and Cr in Molten (Li,Na,K)F

Abstract: The corrosion of structural materials is a great challenge for the applications of a molten salt reactor using molten fluorides. In this paper, electrochemical behavior of pure Fe, Ni and Cr has been investigated in molten (Li,Na,K)F at 973 K by potentiodynamic polarization and electrochemical impedance spectroscopy. The experimental results indicated that three metals are all in active state at the corrosion potential, with an increase in the corrosion potential by the following order: Cr, Fe, Ni. The free corrosion current density of Ni is more than one order of magnitude lower than that of Fe and Cr. A Warburg impedance was observed in the impedance plots for the corrosion of Cr, but not for Ni and Fe. Ni is the most stable metal, then Fe and Cr, and the corrosion of Cr is controlled by the diffusion of oxidants in the melt.

Keywords: Ni, Fe, Cr, molten fluorides, corrosion, electrochemical techniques

PACS® (2010). 61.82.Bg

***Corresponding author: C.L. Zeng:** State Key Laboratory for Corrosion and Protection, Institute of Metal Research, Chinese Academy of Science, Shenyang 110016, China. E-mail: clzeng@imr.ac.cn
Y.X. Xu, Y.L. Wang: State Key Laboratory for Corrosion and Protection, Institute of Metal Research, Chinese Academy of Science, Shenyang 110016, China

1 Introduction

Fluorides are considered for various applications such as thermal storage, electrolyte, coolant or fuel in a molten salt reactor, etc., due to their characteristics of high specific capacity and heat conductivity, good chemical stability at high temperatures, resistance to radiation, capacity to dissolve fission products, etc. [1]. From 1950s the application of molten fluorides as fuel or coolant in a Molten Salt Reactor (MSR) has been taken into consideration [2–4]. However, the corrosion of structural materials in molten fluorides presents a great challenge for the use of molten fluorides in MSR. The corrosion resistance to molten fluorides at high temperatures is a key element for the choice of structural materials. Over the past 60 years, great efforts have been devoted to the issues of materials and corrosion with molten fluoride salts [5–10]. In many high temperature environments, the corrosion resistance of metals or alloys depends on their surface scales among which chromium, aluminium, or silicon oxide scale can provide an excellent protection to alloys. In molten fluorides, however, most oxide films are chemically unstable, and the corrosion occurs through the dissolution of alloying elements into the melts. Alloys whose constituents have less negative free energies of fluoride formation are less prone to corrosion. Thus, more noble materials are suitable for the structural materials of MSR. Ni and some refractory metals such as Mo and W possess higher chemical stability in molten fluorides than Cr, Al and Fe [7]. Some Ni-based alloys with low Cr are considered as the most suitable structure materials for MSR, among which Hastelloy-N (Ni-17%Mo-7%Cr-5%Fe, mass percent) developed by ORNL (Oak Ridge National Laboratory-USA) exhibits great potential for long-term application [11].

Impurities such as H_2O and oxides, temperature gradient and galvanic corrosion have been considered as the main driving forces for the corrosion in molten fluorides [12, 13]. As a main oxidizing impurity, H_2O can react with the fluoride ions to generate HF that then attacks metals to form metal fluorides.

The corrosion processes in molten fluorides are electrochemical in nature, and thereby the electrochemical investigation of corrosion helps to have a better understanding of the corrosion mechanism. Some electrochemical techniques have been applied successfully in the study of the corrosion in molten fluorides [14–17], but with emphasis on the determination of oxidation states, suitable electrode materials and basic electrochemical characteristics of specific elements using cyclic voltammetry [17]. Dasher et al. [14] investigated the compatibility of LiF-NaF-KF salts with oxide dispersion strengthened (ODS) iron-chromium steels and tantalum by a custom designed electrochemical impedance spectroscopy apparatus, and observed that ODS steel/coolant interfacial resistance increased from 873 to 1073 K due to an aluminum-enriched layer forming at the surface. A further increase in temperature to 1173 K caused this layer to break up and

aggressive attack to occur. Ludwig et al. [16] developed an in-situ electrochemical probe utilizing anodic stripping voltammetry (ASV) to measure the dissolved Cr content in molten (Li,Na,K)F. In an electrochemical study of the corrosion of pure metals in molten fluorides, Fabre et al. observed that the corrosion behavior of Ni, Mo and W is different from that of Fe, probably due to their different corrosion mechanisms or a different number of exchanged electrons.

In this paper, potentiodynamic polarization and electrochemical impedance spectroscopy were employed to examine the corrosion of three pure metals Ni, Fe and Cr in molten (Li,Na,K)F at 973 K in air.

2 Experimental procedure

The materials used in the present study are pure Ni, Fe and Cr. The bulk metals were cut into specimens with a size of 5 mm × 30 mm × 2 mm by an electric spark cutting machine, followed by grinding down to 1000 grit SiC paper and cleaning with distilled water and ethanol. A Fe-Cr wire was spot-welded to one end of the specimen for electric connection. The specimen was sealed in an alumina tube with high temperature cement, with a length of 15 mm exposed. The cement was dried at room temperature for 24 h and then at 423 K for 2 h.

Potentiodynamic polarization and electrochemical impedance measurements were undertook in a eutectic 46.5%LiF-11.5%NaF-42%KF (mole percent) at 973 K in Ar with the Princeton Applied Research PARSTAT 2273 potentiostat/Galvanostat. Potentiodynamic polarization was conducted at a scan rate of 20 mV·min^{-1} using a three-electrode system with a Ni/NiF_2 electrode as the reference electrode and a graphite plate as the counter electrode. Electrochemical impedance measurements were undertook at open-circuit potential between 0.01 and 1×10^5 Hz using a two-electrode system composed of two working electrodes. The amplitude of input sine-wave voltage was 10 mV.

All experiments were conducted in a closed stainless steel chamber under a circulating high-purity argon, as shown in Fig. 1. After drying LiF, NaF and KF, respectively, a mixture of (Li,Na,K)F was prepared and then put into a graphite crucible. After drying the mixed salts at 473 K in the reaction chamber under vacuum, the furnace was heated to the experimental temperature of 973 K under the protection of Ar, and the electrode was dipped into the melt to begin the electrochemical experiments.

After electrochemical measurements, the metallurgical sections of the corroded samples mounted in epoxy resin were prepared using kerosene as coolant for grinding and polishing, and then examined by scanning electron microscopy (SEM) coupled with energy dispersive X-ray microanalysis (EDX).

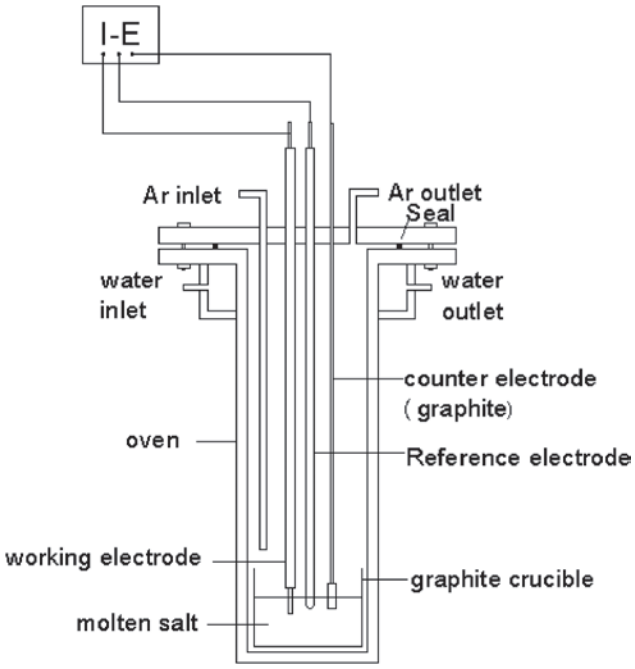

Fig. 1: A schematic diagram of experimental setup

3 Results and discussion

3.1 Potentiodynamic curves

Fig. 2 gives the potentiodynamic curves of Ni, Fe and Cr in molten (Li,Na,K)F at 973 K. Three metals are all in active state at the corrosion potential. Passivation has not occurred for both Ni and Fe, while a "passive region" was observed for Cr, probably due to the enrichment of the dissolved Cr at the surface. With a further increase in the potential, the polarization current of Cr tended to increase again, probably due to the oxidation of Cr^{2+} to form Cr^{3+} [16]. Based on the polarization curves, the corrosion potential (E_{corr}) and free corrosion current density (i_{corr}) were obtained and listed in Table 1. The corrosion potential of Ni is about –0.077 V vs. Ni/NiF_2 much higher than –0.338 V vs. Ni/NiF_2 for Fe and –0.503 V vs. Ni/NiF_2 for Cr. Meanwhile, the corrosion current density of pure Ni is more than one order of magnitude lower than that of Fe and Cr. Ni is the most stable metal, while Cr has the worst corrosion resistance.

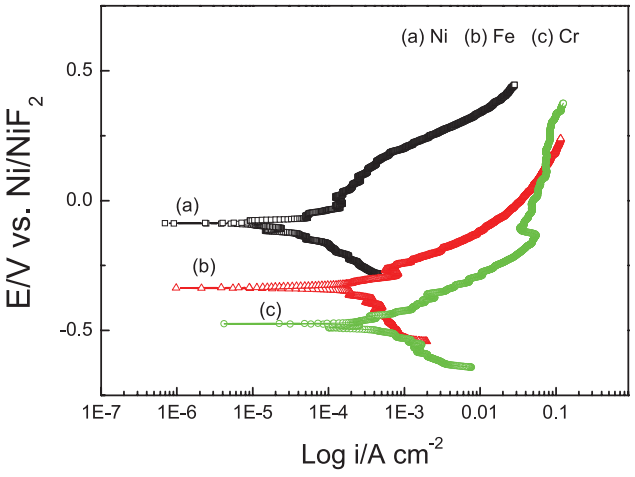

Fig. 2: Potentiodynamic polarization curves for Ni, Cr and Fe in molten (Li,Na,K)F at 973 K

Table 1: Fitting results of polarization curves for Ni, Cr and Fe in molten (Li,Na,K)F at 973 K

	E_{corr} (V vs. Ni/NiF_2)	I_{corr} (μA/cm²)	Corrosion rate (mm/year)
Ni	−0.077	19.3	0.208
Fe	−0.338	261	3.05
Cr	−0.507	494	5.81

3.2 Electrochemical impedance measurements

Fig. 3 gives the typical Nyquist and Bode plots of pure iron after corrosion in the melt for various times. The Nyquist plots are composed of a capacitive loop, with small impedance values that tend to decrease with exposure time.

Fig. 4 shows the typical Nyquist and Bode plots of pure nickel after corrosion in the melt for various lengths of time. Just observed for Fe, the Nyquist plots for the corrosion of Ni are also composed of a capacitive loop, but with significantly larger impedance values.

Unlike Fe and Ni, the Nyquist plots (Fig. 5) for the corrosion of Cr in the melt consist of a small capacitive loop at high frequencies and a line at low-frequency port suggesting a diffusion-controlled reaction.

The impedance spectra for the corrosion of both Ni and Fe, and that for Cr can be fitted using equivalent circuits shown in Fig. 6a and 6b, respectively, where R_s is the molten salt resistance, C_{dl} the double-layer capacitance at the metal/melt interface, R_t the electrochemical transfer resistance, and Z_w the Warburg impedance. In the fitting procedures, C_{dl} is replaced with the constant phase element (CPE) Q_{dl}. The impedance of CPE is expressed as

$$Z_{CPE} = \frac{1}{Y_0(j\omega)^n} \tag{1}$$

Thus, the impedance Z of Fig. 6(a) can be expressed by Eq. (2), and that of Fig. 6(b) by Eq. (3)

$$Z = R_s + \frac{1}{Y_{dl}(j\omega)^{n_{dl}} + \frac{1}{R_t}} \tag{2}$$

$$Z = R_s + \frac{1}{Y_{dl}(j\omega)^{n_{dl}} + \frac{1}{R_t + Z_w}} \tag{3}$$

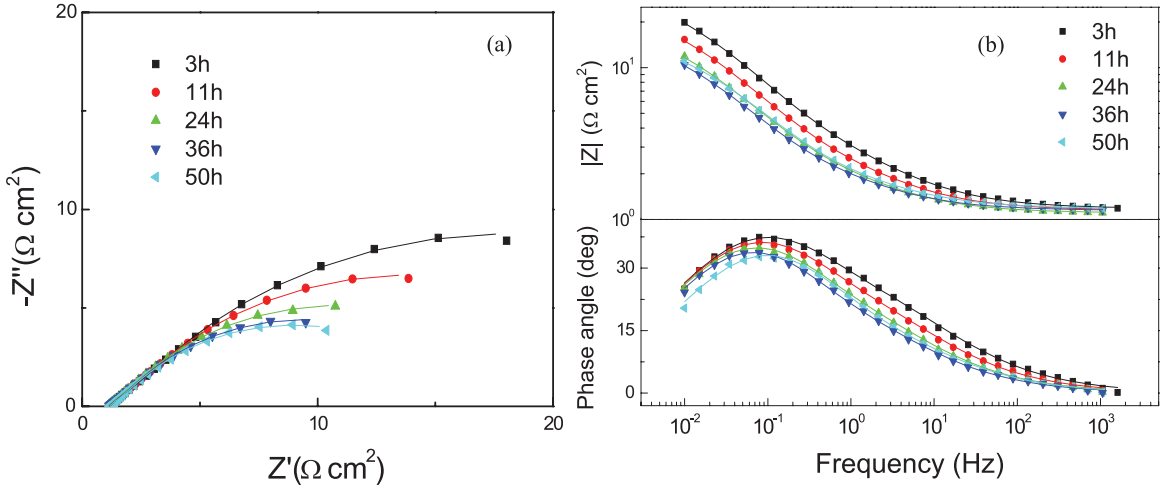

Fig. 3: Nyquist (a) and Bode (b) diagrams of pure iron in molten (Li,Na,K)F at 973 K (Symbol: experimental data; Line: fitted data)

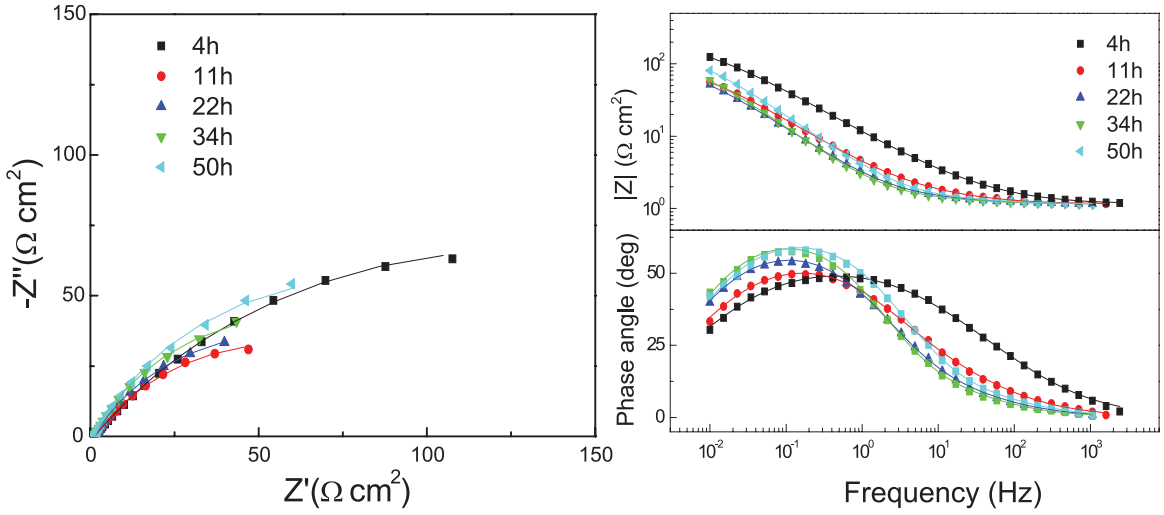

Fig. 4: Nyquist (a) and Bode (b) diagrams of pure nickel in molten (Li,Na,K)F at 973 K (Symbol: experimental data; Line: fitted data)

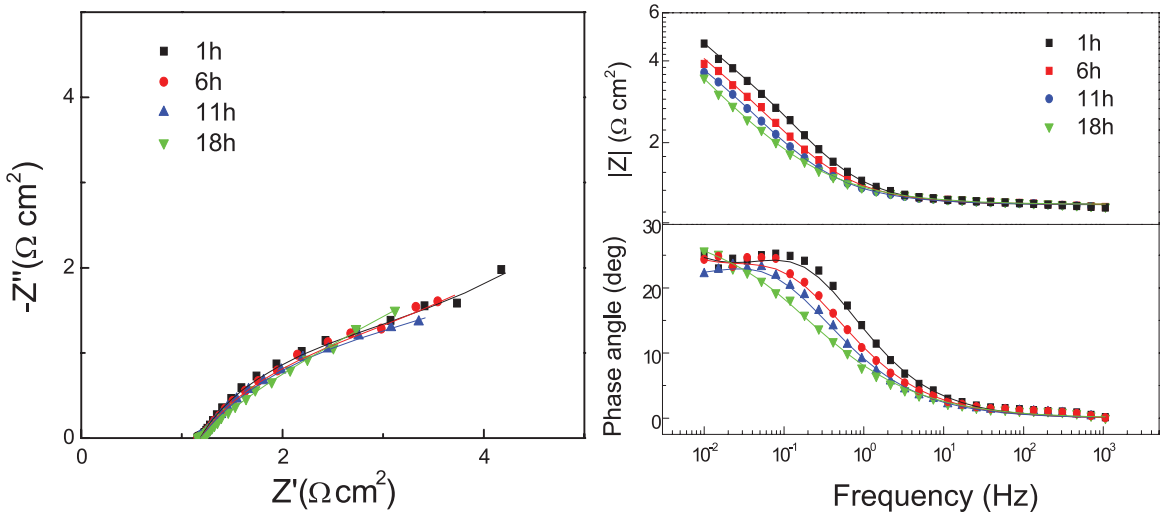

Fig. 5: Nyquist (a) and Bode (b) diagrams of pure chromium in molten (Li,Na,K)F at 973 K (Symbol: experimental data; Line: fitted data)

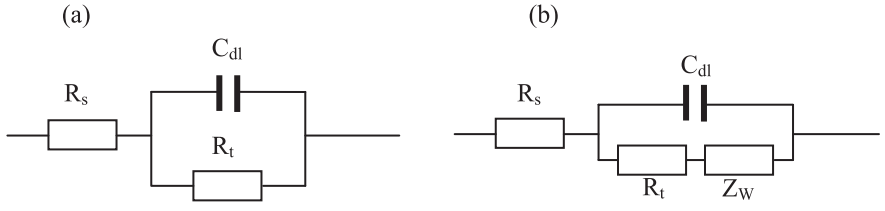

Fig. 6: Equivalent circuits fitting the impedance spectra for the corrosion of both Fe and Ni (a) and of Cr (b)

where Y_{dl} and n_{dl} are constants representing the element Q_{dl}.

The Warburg impedance Z_w is expressed by Eq. (4)

$$Z_w = A_w(j\omega)^{-1/2} \quad (4)$$

where A_w is the coefficient of Z_w.

Based on the equivalent circuits of Fig. 6, the impedance spectra for the corrosion of Fe, Ni and Cr are fitted and the parameters in Eqs. 1–4 are listed in Tables 2–4. Figs. 3–5 show clearly that the fitting results are rather good, suggesting that the proposed equivalent circuits are reasonable.

Table 2: Fitting results of electrochemical impedance spectra for the corrosion of pure iron in molten (Li,Na,K)F at 973 K

Time (h)	R_s ($\Omega \cdot cm^2$)	Y_{dl} ($s^{-n} \cdot \Omega^{-1} \cdot cm^{-2}$)	n_{dl}	R_t ($\Omega \cdot cm^2$)
1	1.107	0.1644	0.5388	46.41
7	1.180	0.1823	0.5457	38.09
11	1.108	0.2313	0.5488	37.86
17	1.107	0.2555	0.5517	28.32
24	1.107	0.2941	0.5544	24.83
36	1.150	0.3377	0.5596	20.91
40	1.109	0.3697	0.5617	19.02
50	1.190	0.2847	0.5696	18.21

Table 3: Fitting results of electrochemical impedance spectra for the corrosion of pure nickel in molten (Li,Na,K)F at 973 K

Time (h)	R_s ($\Omega \cdot cm^2$)	Y_{dl} ($s^{-n} \cdot \Omega^{-1} \cdot cm^{-2}$)	n_{dl}	R_t ($\Omega \cdot cm^2$)
2	1.142	0.0268	0.5589	368.4
7	1.171	0.0528	0.6207	148.7
11	1.182	0.0780	0.6445	130.3
16	1.181	0.1069	0.6794	98.31
22	1.188	0.1075	0.7056	125.4
30	1.184	0.1046	0.7153	127.8
38	1.163	0.1092	0.7318	150.6
50	1.165	0.0742	0.7424	172.8

Table 4: Fitting results of electrochemical impedance spectra for the corrosion of pure Cr in molten (Li,Na,K)F at 973 K

Time (h)	R_s ($\Omega \cdot cm^2$)	$Y_{0,dl}$ ($s^{-n} \cdot \Omega^{-1} \cdot cm^{-2}$)	n_{dl}	R_t ($\Omega \cdot cm^2$)	A_w ($\Omega \cdot cm^2 S^{0.5}$)
1	1.182	0.6183	0.7193	2.801	0.581
4	1.181	0.6675	0.617	3.172	0.730
6	1.186	0.8645	0.6774	2.954	0.485
11	1.185	1.109	0.6471	3.448	0.309
15	1.187	1.254	0.6249	3.61	0.403
18	1.184	1.34	0.5597	5.039	0.551

Tables 2–4 indicate that the parameter R_t for the corrosion of pure Ni has the largest values, then Fe and Cr, suggesting that the corrosion resistance of three metals ranks as follows: Ni > Fe > Cr. Differing from pure Ni and Fe, the corrosion of pure Cr is determined by the diffusion of oxidants in the melt, with the highest corrosion rate. The impedance results are in a good agreement with the potentiodynamic polarization results.

3.3 Characterizations of the corroded samples

Fig. 7 shows the cross-sectional morphology of pure Fe after immersion in the melt for 50 h. The corrosion of Fe occurs through the dissolution of Fe into the melt, without the formation of a scale.

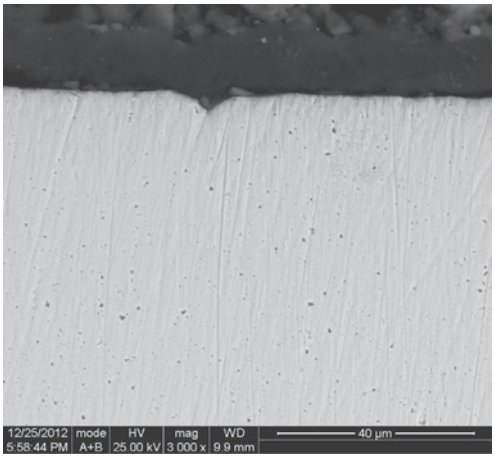

Fig. 7: Cross-sectional morphology of pure iron after immersion in molten (Li,Na,K)F at 973 K for 50 h.

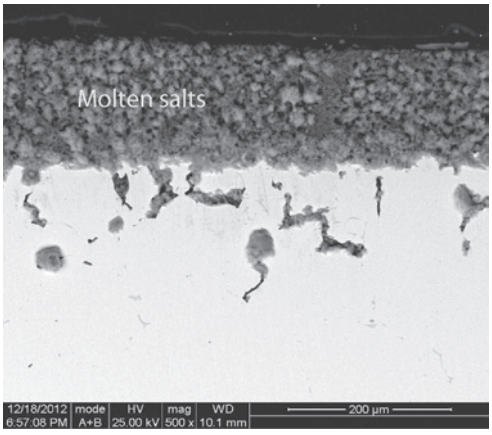

Fig. 8: Cross-sectional morphology of pure Nickel after immersion in molten (Li,Na,K)F at 973 K for 50 h.

Fig. 8 gives the cross-sectional morphology of pure Ni after corrosion in the melt for 50 h. Unlike Fe, pure Ni goes through non-uniform dissolution with an attack depth of around 200 µm, forming some internal voids filled with some fluorides. This non-uniform corrosion may be related to the presence of impurities such as Co, Fe, etc in the Ni substrate. These impurity compounds along the grain boundaries have less chemical stability than Ni, and thus may be attacked preferentially.

As compared to Fe and Ni, Cr was attacked more severely. Fig. 9 presents the cross-sectional morphologies of Cr corroded in the melt for 18 h. The corrosion at the melt/gas interface is significantly severer than in the melt. It was also noted that some Cr-rich oxides were observed in the salts left on the specimen surface, probably

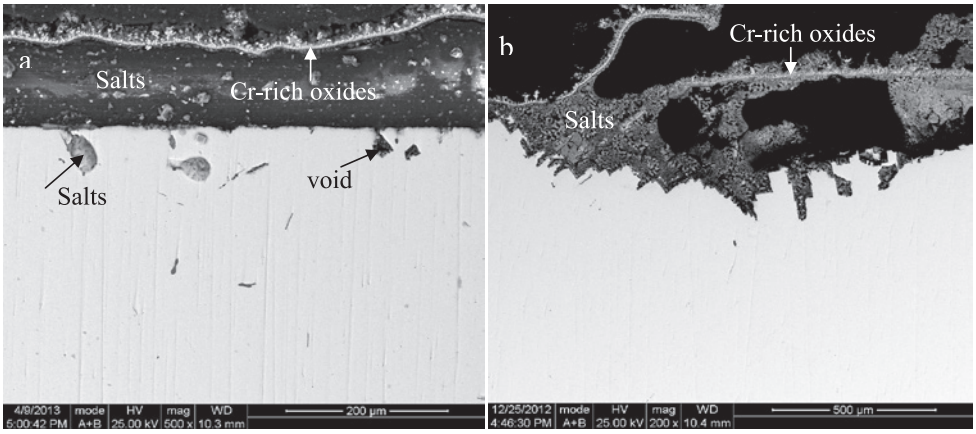

Fig. 9: Cross-sectional morphologies of pure chromium after immersion in molten (Li,Na,K)F at 973 K for 18 h. (a) Cr corroded in the melt; (b) Cr corroded at the melt/gas interface

resulting from the reaction between the fluorides, especially CrF_2 generated from the dissolution of Cr in the melt, and some impurities such as H_2O and O_2 in Ar. Moreover, localized corrosion has also developed deep into the substrate, forming some voids that are filled with fluorides.

3.4 Discussion

The above results indicate clearly that Ni, Fe and Cr suffer from active dissolution in molten (Li,Na,K)F, with a corrosion resistance order of Ni > Fe > Cr. Moreover, the corrosion of pure Cr exhibits the features of a diffusion-controlled reaction.

Most oxide films formed on alloy surface at high temperatures in an oxidizing environment are chemically unstable in molten fluorides, and thus corrosion occurs through the thermodynamically driven dissolution of alloying elements into the melts. In the present environments, the main driving force for the corrosion of three pure metals is impurities such as H_2O mainly coming from fluoride salts and Ar gas. From the viewpoint of corrosion, H_2O and oxides are among the most deleterious impurities in molten fluorides. As common impurities, however, H_2O and oxides are extremely hard to be removed completely. At high temperatures, H_2O may react with fluorides to generate gaseous HF:

$$MF(l) + H_2O(g) = MOH(l) + HF(g) \quad (5)$$

$$2MF(l) + H_2O(g) = M_2O(l) + 2HF(g) \quad M = Li, Na, K \quad (6)$$

The generated HF may be dissolved partially into the melt and attack metals. The corrosion of metals or alloys comprises oxidation and reduction processes. The anodic oxidation and cathodic reduction reaction can be expressed by Eqs. (7) and (8), respectively:

$$Me = Me^{n+} + ne^- \quad (7)$$

$$HF(l) + e = F^- + \frac{1}{2}H_2 \quad M = Fe, Ni, Cr \quad (8)$$

The general reaction can be expressed by Eq. (9).

$$M + n \cdot HF(l) = MF_n + \frac{n}{2}H_2(g) \quad (9)$$

Based on the thermodynamic data, the standard Gibbs free energy and standard potential of Eq. (9) for three metals have been calculated, and are listed in Table 5.

Table 5 shows clearly that the chemical stability of three metals increases in the following order: Cr, Fe, Ni. These theoretical results are in a good agreement with the electrochemical results. The thermodynamic and experimental results confirm that Ni exhibits the best corrosion resistance, then Fe and Cr.

Table 5: Standard Gibbs energy, $\Delta G^0_{Me/Me^{n+}}$ and standard potential, $E^0_{(Me/Me^{n+})vs.(HF/H_2)}$ for the dissolution of pure metals into metal fluorides at 973 K

Metal (M)	Reactions	$\Delta G^o_{Me/Mey+}$ (kJ mol^{-1})	$E^o_{(Me/Mey+)\ vs.\ (HF/H2)}$ (V)
Ni	$Ni + 2HF(l) = NiF_2 + H_2(g)$	−64.334	−0.333
Fe	$Fe + 2HF(l) = FeF_2 + H_2(g)$	−131.981	−0.684
Cr	$Cr + 2HF(l) = CrF_2 + H_2(g)$	−211.982	−1.098

As the corrosion of Cr is determined by the diffusion of oxidants in the melt, it is attempted to calculate the solubility of oxidants in the melt using diffusion impedance. According to the theory of ac impedance for an electrode, the Warburg coefficient, A_w, under the conditions of semi-infinite diffusion is given by Eq. (10) [19].

$$A_w = \sum \frac{RT}{n_i^2 F^2} \left(\frac{1}{C_i \sqrt{D_i}}\right) \tag{10}$$

where i denotes the diffusion species, n_i the electron number per molecule of species i when reduced, F the Faraday constant, and C_i and D_i the solubility and the diffusion coefficient of species i. In molten fluorides, the main oxidizing species are said to be H_2O and HF. Traces of water are unstable in molten fluorides because it reacts with the fluoride ions to generate HF. Thereby, in the present study, the diffusion species HF involved in reduction reaction is under consideration. Therefore, Eq. (10) can be simplified to

$$A_w = \frac{RT}{n_{HF}^2 F^2} \left(\frac{1}{C_{HF} \sqrt{D_{HF}}}\right) \tag{11}$$

Introducing the value of $A_w = 0.551\ \Omega \cdot cm^2 \cdot s^{0.5}$ for Cr corroded for 18 h, and other parameters into Eq. (11), then the experimental value of $C_{HF}\sqrt{D_{HF}}$ can be calculated to be 1.57×10^{-6} mol/cm^2·s$^{0.5}$. The diffusion coefficients of species in molten salts are generally in the range $1 \sim 8 \times 10^{-5}$ cm^2·s^{-1} [20]. Assuming $D_{HF} = 8 \times 10^{-5}$ cm^2·s^{-1}, then the value of C_{HF} in molten (Li,Na,K)F can be calculated to be 1.76×10^{-4} mol·cm^{-3} (around 1740 ppm). The relatively high content of HF suggests the presence of a high content of H_2O in the experimental environments. After impedance measurements, the corroded Cr was lifted above the melt, and then cooled with furnace. During this process, the fluorides left on the surface of Cr may react with H_2O to form metal oxides. Because chromium fluorides are present in the melt, it is thermodynamically possible to form Cr-rich oxides in the residual fluorides on Cr. The experimental results prove that these Cr-rich oxides mainly exist in the outer part of the residual salt layer. Decreasing the impurity H_2O helps to alleviate the corrosiveness of molten fluorides.

4 Conclusion

Pure Fe, Ni and Cr are all in active dissolution state at the corrosion potential. The free corrosion potential of Ni, Fe and Cr is –0.077 V, –0.338 V and –0.507 V vs. Ni/NiF_2, respectively. The free corrosion current density of Ni is 19.3 μA·cm^{-2} more than one order of magnitude lower than 261 μA·cm^{-2} for Fe and 494 μA·cm^{-2} for Cr. The Nyquist plots for the corrosion of both Ni and Fe are composed of a single capacitive loop, while a Warburg impedance is observed in the impedance plots of Cr. The appearance of Warburg impedance suggests that Cr is dissolved rapidly into the melt, and its corrosion is controlled by the diffusion of oxidants in the melt. Based on the Warburg impedance measurements of Cr, the solubility of oxidant species HF is calculated approximately to be the order of 1740 ppm. The corrosion of Ni, Fe and Cr occurs through their dissolution into the melt, and Ni is the most stable metal, then Fe and Cr.

The project was supported by National Natural Science Foundation of China, Grant No. 51271190.

Received: July 25, 2013. Accepted: August 21, 2013.

References

[1] W.R. Grimes, E.G. Bohlmann, A.S. Meyer and I.M. Dale, in: *Molten-Salt Reactor Program,* ORNL-4812, **5**, *Fuel and Coolant Chemistry* (1972), p. 95.
[2] D.F. Williams, L.M. Toth and K.T. Clarno, ORNL/TM-2006/69, Oak Ridge National Laboratory (2006).
[3] W.R. Grimes, in: *Fluid-fueled Reactors*, Chapter 12, edited by H.G. Macpherson, Addision-Wesley, New York (1958), pp. 569–594.
[4] H.E. McCoy Jr., ORNL-TM-5920, Oak Ridge National Laboratory (1978).
[5] J.W. Koger, ORNL TM-4188, Oak Ridge National Laboratory (1972).
[6] D. Williams, L. Toth, and K. Clarno, ORNL/TM-2006/12, United States Department of Energy (2006).
[7] L. Olson, J.W. Ambrosek, K. Sridharan, M.H. Anderson and T.R. Allen, *Journal of Fluorine Chemistry*, **130**, 67–73 (2009).
[8] L. Olson, K. Sridharan, M. Anderson and T. Allen, *Journal of Nuclear Material*, **411**, 51–59 (2011).
[9] L. Olson, K. Sridharan, M. Anderson and T. Allen, *Materials at High Temperatures*, **27**, 145–149 (2010).
[10] P. Sabharwall, M. Ebner, M. Sohal, P. Sharpe, M. Anderson, K. Sridharan, J. Ambrosek, L. Olson and P. Brooks, INL/EXT-10-18090, Idaho National Laboratory (2010).
[11] W.R. Grimes, in: *Fluid Fuel Reactors*, Chap. 13, edited by H. G. Macpherson, Addison-Wesley, New York (1958), pp. 595–625.
[12] J.H. Devan, ORNL-TM-2021, Oak Ridge National Laboratory (1969).
[13] L.C. Olson, *Materials Corrosion in Molten LiF-NaF-KF Eutectic Salt*, University of Wisconsin-Madison, Doctor thesis (2009), p. 13.

[14] B. El-Dasher, J. Farmer, J. Ferreira, M.S. de Caro, A. Rubenchik and A. Kimura, *Journal of Nuclear Materials*, **419**, 15–23 (2011).
[15] S. Fabre, C. Cabet, L. Cassayre, P. Chamelot, J. Finne, D. Noel and P. Taxil, *High Temperature Corrosion and Protection of Materials 7*, **595–598**, 483–490 (2008).
[16] D. Ludwig, L. Olson, K. Sridharan, M. Anderson and T. Allen, *Corrosion Engineering, Science and Technology*, **46**, 360–364 (2011).
[17] W. Grimes, E. Bohlmann, A. Meyer, J. Dale, ORNL-4812, Oak Ridge National Laboratory, Oak Ridge, TN, USA (1972).
[18] J.F. Qiu, *Rare Metal Materials and Engineering*, **2**, 64 (1992).
[19] G.M. Schmid, *Electrochimica Acta*, **15**, 65–71 (1970).
[20] A. Klemm, In: *Molten Salt Chemistry*, edited by M. Blander, Wiley, New York (1964), p. 535.